journal

J. Am. Ceram. Soc., 91 [4] 1300–1305 (2008)
DOI: 10.1111/j.1551-2916.2008.02311.x

Incorporation of Galvanic Waste (Cr, Ni, Cu, Zn, Pb) in a Soda–Lime–Borosilicate Glass

Antonio C. Silva and Sonia Mello-Castanho

IPEN, Energy and Nuclear Research Institute, São Paulo, Brazil

Francisco Guitian

Instituto de Cerámica de Galicia, Universidad de Santiago de Compostela, Santiago de Compostela, Spain

Isabel Montero, Antonio Esteban-Cubillo, Isabel Sobrados, Jesus Sanz, and Jose S. Moya**,†

Instituto de Ciencia de Materiales de Madrid, Consejo Superior de Investigaciones Cientificas (CSIC), 15263 Madrid, Spain

In the present investigation, a glassing process for galvanic waste (GW) incorporation with a high chemical stability is presented. Glasses with up to 50 wt% of galvanic solid waste by modifications in the basic composition of soda–lime–borosilicate glasses were prepared. After fusing at temperatures up to 1300°C, the glasses were characterized by inductively coupled plasma, scanning electron microscopy/energy-dispersive X-ray spectroscopy, high-temperature microscopy, transmission and reflected light microscopy, nuclear magnetic resonance, X-ray photoelectron spectroscopy, and X-ray diffraction methods. The chemical stability was evaluated by hydrolytic attack assays. Glasses containing up to 40 wt% of GW with a very high chemical stability, similar to bottle glasses, were obtained.

I. Introduction

At present, achievement of sustainable development is widely regarded as a key social, economic, and technical driver, and a key consideration in assessing the relative value and quality of future developments.[1] The sustainable development concept concerns a wide range of actions, but without doubt, one of the most important is the control of hazardous waste emissions into the biosphere. Many of these hazardous wastes contain heavy metals, the presence in the biosphere is considered to be undesirable because of their often-deleterious impact on human health. For instance, the presence of Cr^{3+} in wastes can yield free Cr^{6+}, which is carcinogenic and soluble in water.[1–4]

Waste recycling to its original raw material (primary recycling) is only possible in a limited number of cases. Obtaining a new product from industrial wastes, i.e., secondary recycling is in many cases the best way. Waste-based ceramic products, such as low-technology materials used in road construction, roof tile, cements and concretes, and house brick applications, may be an interesting option[1,5,6]; however, in order to attain higher environmental stability, glass-based ceramic products are the best option.

At present natural glasses contain toxic materials in their structure that have shown environmental inertia through a time span. These elements are absorbed in the chemically stable vitrous matrix.[7] The vitrification process simulates the natural phenomenon of glassing from volcanic rocks (i.e., Basalt) and has been applied industrially for the treatment of radioactive wastes[8] and for the stabilization of ashes from urban garbage incinerators.[5,6,9]

Glass has been used due to its chemical and physical–chemical characteristics such as good behavior during fusion, homogeneity, durability, and stability under several environmental conditions.[7,10] These characteristics can be used for the stabilization of galvanic waste (GW).[11] The production of toxic GW (Cr, Ni, Zn, Cu, Pb) in developed and underdeveloped countries is higher than 1 000 000 ton/year.[4,12] The main objective of the present investigation is to stabilize these toxic heavy metals into an appropriate boro-silicate glassy stable matrix.

II. Experimental Procedure

(1) Starting Materials

Silica, α-quartz, with an average grain size $\approx 10 \pm 3$ μm from the filter sleeve of the milling process of a sanitary industry plant (São Paulo, Brazil); granite sludge with an average grain size $\approx 15 \pm 3$ μm (São Paulo, Brazil); and GW from a metal electroplating plant with an average grain size $\approx 8 \pm 3$ μm (São Paulo, Brazil) were used as raw materials. The corresponding chemical compositions are reported in Table I. The raw materials' chemical compositions were determined by X-ray fluorescence (X-Ray Rix2000, Rigaku Corporation, Tokyo, Japan).

Additionally, the following reagent-grade aluminum oxide (99.9 wt%, Alcoa A-1000, Richmond, VA), sodium hydroxide (NaOH 97.0 wt%, heavy metals ≤ 0.003 wt%, $Cl^- \leq 0.005$ wt%, Fe ≤ 0.001 wt%, Hg ≤ 0.1 ppm, K ≤ 0.02%, $Na_2CO_3 \leq 1.0$ wt%, $NH_4OH \leq 0.02$ wt%, Ni ≤ 0.001 wt%, $PO_4^{3-} \leq 0.001$ wt%, $SO_4^{2-} \leq 0.003$ wt%, absorbed water ≤ 2.0 wt%; Nuclear, São Paulo, Brazil), calcium oxide (CaO 97.0 wt%, heavy metals ≤ 0.005 wt%, $Cl^- \leq 0.05$ wt%, $SO_4^{2-} \leq 0.5$ wt%, Fe ≤ 0.5 wt%, insolubles ≤ 0.01 wt%, absorbed water ≤ 2.0 wt%; Química Moderna, São Paulo, Brazil), potassium carbonate (K_2CO_3 99.0 wt%, heavy metals ≤ 5 ppm, insolubles ≤ 0.01 wt%, SiO_4 0.005 wt%, $PO_4^{3-} \leq 0.001$ wt%, Fe ≤ 5 ppm, $Na_2CO_3 \leq 0.02$ wt%, $NH_4OH \leq 0.01$ wt%, Ca and Mg ppt ≤ 0.01 wt%, $SO_4^{2-} \leq 0.004$ wt%, $Cl^- \leq 0.1$ ppm; Carlo Erba, Rodano, Italy) and boric acid (H_2BO_3 97.0 wt%, $Cl^- \leq 0.005$ wt%, Ca ≤ 0.02 wt%, CH_3OH insolubles ≤ 0.01 wt%, CH_3OH nonvolatile ≤ 0.1 wt%, heavy metals ≤ 0.003, Fe ≤ 0.003 wt%, $PO_4^{3-} \leq 0.01$ wt%, $SO_4^{2-} \leq 0.03$ wt%, and absorbed water ≤ 3.0 wt%; Química Moderna) were also used.

C. Jantzen—contributing editor

Manuscript No. 23402. Received July 2, 2007; approved December 17, 2007.

The authors wish to thank Brazilian State of Sao Paulo Research Foundation (Fapesp) and National Council for Scientific and Technological Development (CNPq/BR), for A.C. Silva 202441/2006-7 and 140581/2005-7 scholarships. This work has been supported by the Spanish Ministry of Education under (Spain) MAT2006-10249-C01-02, and by the Galician Regional Government (Spain) grand PGIDITPXIC23901PN.

†Author to whom correspondence should be addressed. e-mail: jsmoya@icmm.csic.es

**Fellow, The American Ceramic Society.

Table I. Starting Materials X-Ray Fluorescence Analyzed Composition (wt%)

Elements	Silica waste	Granite sludge	Galvanic waste
SiO_2	98.0	72.0	22.0
Al_2O_3	0.9	16.0	0.9
CaO	0.1	0.6	14.0
K_2O	0.2	6.2	0.2
Na_2O	0.2	4.9	1.2
Fe_2O_3	0.2	0.2	1.1
SO_3	0.1	$\leq$0.1	7.4
MnO	—	$\leq$0.1	0.1
Cr_2O_3	—	—	21.0
CuO	—	—	6.9
NiO	—	—	13.0
ZnO	—	—	4.7
PbO	—	—	1.3
MgO	—	—	3.5
Minor elements	0.3	—	2.7
Sum	100.0	100.0	100.0

(2) Glasses' Formulation

In order to avoid Cr, Ni, Cu, and Zn sublimation, the glass formulation was designed taking into account that the glass melting temperature must be $\leq$1300°C.[11] In this regard, five glass compositions (labeled T05, T10, T15, T20, and T25) belonging to a $CaO–Na_2O–SiO_2$ equilibrium diagram (Fig. 1) were used as reference materials.[13] In these compositions, the amount of CaO (R^{2+} glass modifier) ranges from 5 to 25 wt%.

In order to reach the adequate viscosity to cast the melt glass, part of the glass-forming SiO_2 content was replaced by B_2O_3, considering the $B_2O_3–CaO–SiO_2$[14] phase equilibrium diagram (Fig. 2) and keeping the CaO content fixed. As can be observed in this plot, the "liquidus" temperature for these five glasses ranges between 1200° and 1300°C. The new prepared glasses were, respectively, labeled as T05C, T10C, T15C, T20C, and T25C in agreement with its CaO wt% content.

To incorporate the GW into these glass series, the CaO wt% content was replaced in the glass formulation by the transition metal oxides present in the GW, considering the molar equivalence of the more typical valence of the transition metals present in the waste (Cr^{3+}, Ni^{2+}, Zn^{2+}, Ca^{2+}, Pb^{2+}) versus the Ca^{2+} (i.e., 1.0 mol Cr^{3+} is equivalent to 1.5 mol Ca^{2+}; 1.0 mol Ni^{2+} is equivalent to 1.0 mol Ca^{2+}). The glasses prepared with GW additions (R) were, respectively, labeled as T05R, T10R, T15R, T20R, and T25R. The final glass calculated compositions are reported in Table II. The different glass compositions were homogenized in an agate mortar and subsequently melted into an alumina crucible at 1300°C for 2 h in a vertical electric furnace. The glasses were cast into bar molds of ($10 \times 10 \times 50$) mm and then annealed at 500°C for 2 h.

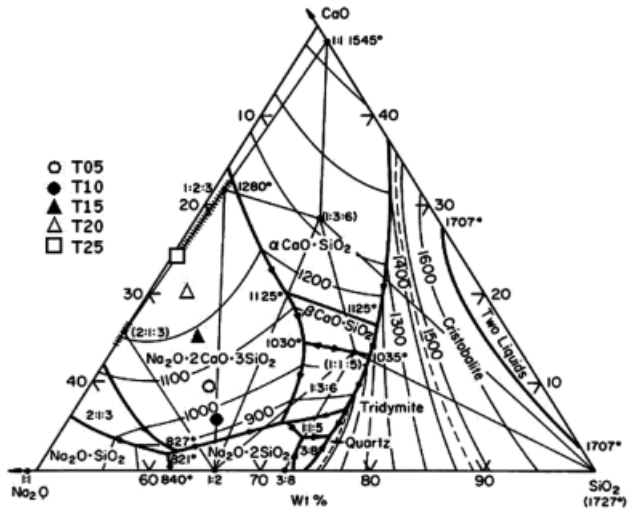

Fig. 1. $CaO–Na_2O–SiO_2$ equilibrium diagram[13] with indication of the selected glass compositions.

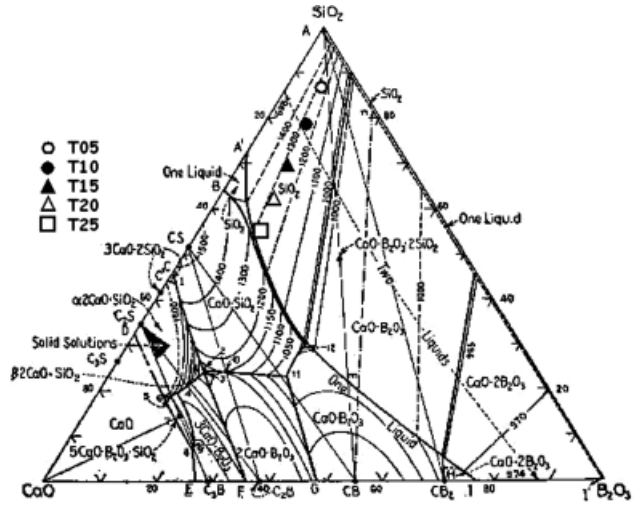

Fig. 2. $B_2O_3–CaO–SiO_2$ equilibrium diagram[14] with indication of the selected glass compositions.

The corrosion of alumina crucibles by molten glass is a well-studied phenomenon; additionally, transition metals' high-content molten glasses are also very corrosive to Pt crucibles.[15,16] In this sense, alumina crucibles were selected in this study as a more acceptable source of sample contamination and also because of its low cost.

The final glasses were studied by X-ray diffraction (XRD) (Bruker AXS D8—Advance diffractometer, Madison, WI), transmission and reflected light optical microscopy (Leica Microsystems GmbH—DM RM, Heerbrugg, Switzerland), nuclear magnetic resonance (MAS-NMR) (Advance 400–9.4 Tesla, Bruker, Karlsruhe, Germany), high-temperature microscopy (Hesse Instruments, Osterode am Harz, Germany), scanning electron microscopy/energy-dispersive X-ray scanning (SEM-EDS) (Jeol 6400, Jeol Ltd., Tokyo, Japan; INCA, Oxford Instruments, Abingdon, Oxfordshire, U.K.), and X-ray photoelectron spectroscopy (XPS) (VGS ESCALAB 210, Seoul, Korea), with a nonmonochromatic Mg$K\alpha$ X-ray source ($h\nu = 1253.6$ eV); and combined resolution of the analyzer and the $K\alpha$1,2 line was 0.75 eV, and the oxide composition was determined by inductively coupled plasma (ICP) spectrometry (Varian Inc. Liberty 2000, Palo Alto, CA).

The chemical resistance of the obtained glasses was evaluated by both a static test, i.e. the PCT-B method (ASTM 1285–02),[17] and a dynamic test, i.e. hydrolytic resistance method. The PCT-B was performed with crushed samples ($d_{50} = 28 \pm 0.3$ μm) immersed in ultrapure water for 7 days at 90°C, as the ASTM 1285–02 norm and the leachate were analyzed by ICP.

The hydrolytic resistance of the glasses was evaluated from the weight loss of bulk samples continually washed by distillated water at about 90°C, using the method described by Day *et al.*[18] and modified using a Soxhlet distillation column.[11] In this method, samples ($1 \times 1 \times 0.1$ cm^3) were cut from glassy rectangular bars. The surfaces were ground using 240 grit SiC paper with oil as the cooling agent and then washed ultrasonically in acetone (PA Merck, São Paulo, Brazil) for 15 min, dried at 110°C for 2 h, cooled in a desiccator, and then weighed ($\pm$0.01 mg). This washing procedure (except for ultrasonic washing) was followed before each weighing during the corrosion test.

The assay was performed in a borosilicate glassware (Pyrex®, Corning Incorporated, Corning, NY) Soxhlet apparatus with 500 ml of deionized water at boiling temperature. A dynamic condition (Soxhlet) was chosen to avoid dissolved species;

Table II. Glass Calculated Compositions (wt%)

	Compositions									
	T05C	T05R	T10C	T10R	T15C	T15R	T20C	T20R	T25C	T25R
SiO_2	56.3	55.1	52.2	49.8	46.7	43.6	42.6	38.9	38.2	34.2
B_2O_3	4.2	4.1	5.4	5.2	6.8	6.3	7.8	7.2	9.2	8.2
Na_2O	30.0	29.3	28.0	26.8	27.0	25.2	25.0	22.8	23.0	20.6
CaO	4.8	1.4	9.8	2.7	14.6	3.9	19.5	5.1	24.4	6.2
K_2O	1.0	1.0	1.0	0.9	1.0	0.9	1.0	0.9	1.0	0.9
Al_2O_3	2.0	1.9	2.0	1.9	2.0	1.8	2.0	1.8	2.0	1.7
MgO	0.0	0.3	0.0	0.7	0.0	1.0	0.0	1.3	0.0	1.5
Cr_2O_3	0.0	2.0	0.0	3.9	0.0	5.8	0.0	7.6	0.0	9.3
NiO	0.0	1.2	0.0	2.4	0.0	3.6	0.0	4.7	0.0	5.7
CuO	0.0	0.7	0.0	1.3	0.0	1.9	0.0	2.5	0.0	3.0
ZnO	0.0	0.4	0.0	0.9	0.0	1.3	0.0	1.7	0.0	2.1
PbO	0.0	0.1	0.0	0.2	0.0	0.4	0.0	0.5	0.0	0.6
Fe_2O_3	0.1	0.2	0.1	0.3	0.1	0.4	0.1	0.5	0.1	0.6
SO_3	0.1	0.8	0.1	1.4	0.1	2.1	0.0	2.7	0.0	3.3
Others	1.5	1.5	1.4	1.6	1.7	1.8	2.0	1.8	2.1	2.0
Sum	100.0	100.0	100.0	100.0	100.0	100.0	100.0	100.0	100.0	100.0

interference in the corrosion process, and maintain the driving force for leaching. In this process the samples were continually washed with distillated water and species dissolved from the glass samples were carried with the leaching solution to the boiler recipient.

The leachate solution was completed at 24, 72, 168, and 336 h with deionized water when the sample was removed for weighing. The weight loss of the sample was measured at each time interval. All tests were performed in duplicate.

The dissolution rate (DR) of bulk samples was calculated from the measured weight loss, δW (g), sample surface area, SA (cm^2), and the immersion time, t (min), using the following equation:

$$DR = (W_i - W_f)/(SA \times t)$$

III. Results and Discussion

(1) Structure of Glasses

The XRD patterns corresponding to T05C, T10C, T15C, T20C, and T25C indicate only the presence of a glassy phase (data not shown). The XRD patterns corresponding to T05R, T10R, T15R, T20R, and T25R samples are shown in Figs. 3 and 4. In general, XRD patterns are formed by broad components; however, in T20R and T25R glasses, Ni_3S_2, Cu_2S, or Cr_2O_3 crystalline phases were also detected (Fig. 3).

In the case of T25R glass, spherical inclusions of 1–3 mm diameter are observed at the bulk of the glass bars. These inclusions were studied by XRD and SEM-EDS. The corresponding XRD pattern (Fig. 4) shows that the inclusions are constituted by Ni_3S_2 and Cu_2S. The SEM micrograph and the EDS patterns corresponding to the inclusion polish surface (data not shown) show dendritic precipitates of Cu_2S into a Ni_3S_2–Cu_2S liquid phase. Then, these glass-insoluble inclusions[19] were formed by segregation of a Ni_3S_2–Cu_2S melt during cooling at temperatures ranging from 1000° to 725°C, as indicated by the Ni_3S_2–Cu_2S equilibrium diagram.[20]

Table III shows a negligible loss of transition metals in the glasses obtained. These results were normalized, considering the expected Al_2O_3 fraction incorporated into the glass from the crucible, as a reference.

In Fig. 5, a transmission optical micrograph obtained by using a thin glass layer (≈30 μm) of the T20R glass is shown. In this picture, green cromite hexagonal plates embedded in a glassy matrix can be observed. This result is consistent with the SEM-EDS observations of T20R. The EDS analyses of the T20R glassy matrix showed a significant decrease of the chromium content (from 7.6 to 2.2 wt%), with respect to T20R nominal composition (Table III). Although SO_3 amounts were included in the table of calculated composition, SO_3 was not detected in the glass chemical analyses. Additionally, SO_3

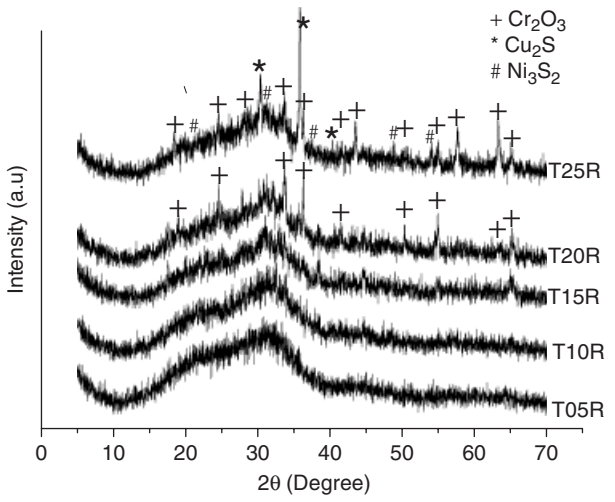

Fig. 3. X-ray diffraction patterns corresponding to T05R, T10R, T15R, T20R, and T25R compositions.

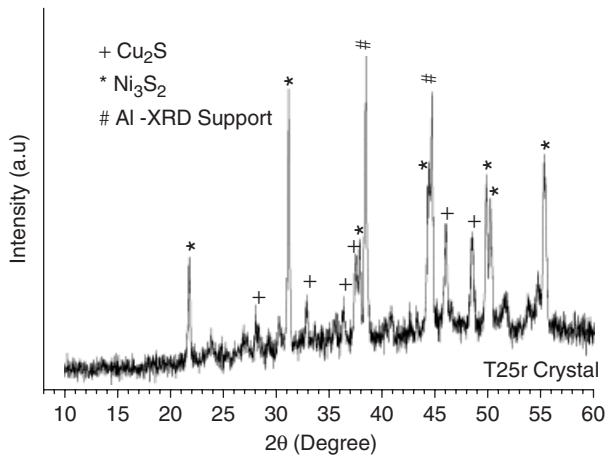

Fig. 4. X-ray diffraction pattern corresponding to T25R inclusion.

Table III. Chemical Analyses (ICP) of T15R and T20R Glasses

	T15R		T20R	
Oxide	Calculated	By ICP	Calculated	By ICP
SiO_2	43.60	36.00	38.90	39.40
B_2O_3	6.30	5.98	7.20	6.93
Na_2O	25.20	32.20	22.80	22.60
CaO	3.90	4.13	5.10	5.64
K_2O	0.90	0.32	0.90	0.36
Al_2O_3	1.80	8.01	1.80	6.67
MgO	1.00	1.07	1.30	1.41
Cr_2O_3	5.80	5.07 (5.58)*	7.60	6.72 (7.40)*
NiO	3.60	2.23 (2.45)*	4.70	3.08 (3.39)*
CuO	1.90	0.91 (1.0)*	2.50	1.14 (1.26)*
ZnO	1.30	0.80 (0.88)*	1.70	1.12 (1.23)*
PbO	0.40	0.10 (0.11)*	0.50	0.13 (0.14)*
Fe_2O_3	0.40	0.25	0.50	0.32
TiO_2	—	0.04	—	0.05
MnO_2	—	0.03	—	0.05
SO_3	2.10	—	2.70	—
Others	1.80	2.86	1.80	4.38

*Normalized value considering the incorporated alumina from the crucible.

determination was not performed in T25R glass because the presence of inhomogeneously distributed copper sulfide and nickel sulfide nodules in the glass made it impossible to obtain a representative sample of glass to confirm the sulfur content of the glass.

The local structure of glasses has been assessed by MAS-NMR spectroscopy. The ^{29}Si MAS-NMR spectra of glasses are formed by a central component and several spinning side bands, separated by the rotation rate expressed in c/s. In T10C and T20C glasses, the main detected component at −86.5 ppm corresponds to Si in tetrahedral chain arrangements (Q^2 environments) (Fig. 6). In T10R and T20R glasses, the intensity and linewidth of the different components increase considerably as a consequence of paramagnetic-incorporated atoms. In T20R, the main signal is shifted to −90 ppm and a new component at −110 ppm, ascribed to the silica segregation, is detected.

The ^{11}B MAS-NMR spectra of glasses formed by two components at 17 ppm and a single component at 0.1 ppm have been assigned, respectively, to B atoms in trigonal and tetrahedral coordination (Fig. 7). The presence of paramagnetic cations in T10R and T20R glasses again leads to an increase of the intensity and linewidth of the components. In general, it is observed that trigonal B lines increase with the amount of calcium and metal transition elements.

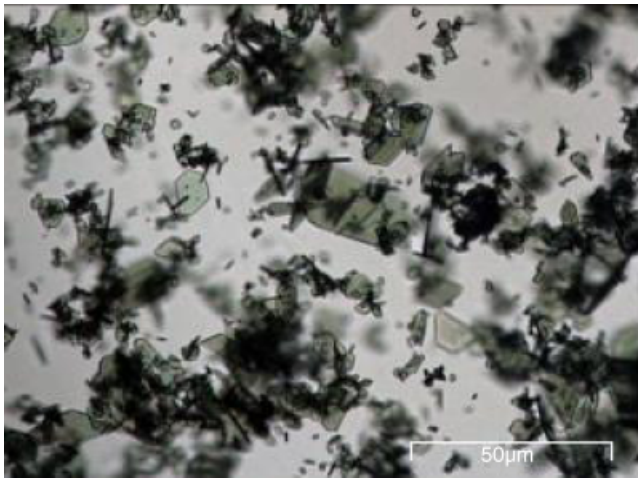

Fig. 5. T20R optical transmission micrograph.

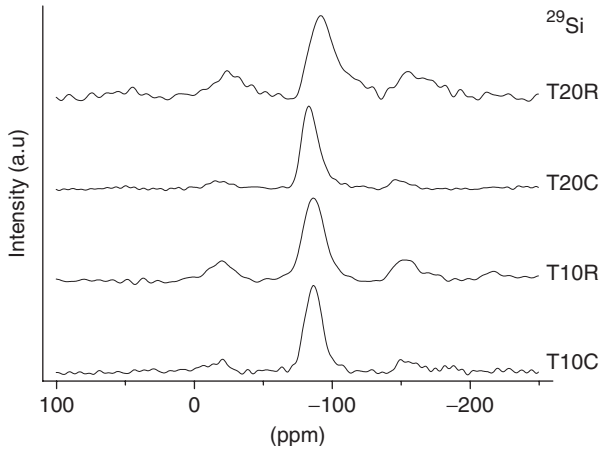

Fig. 6. ^{29}Si MAS-NMR spectra for T10C, T10R, T20C, and T20R glasses.

Glasses were characterized by XPS. Figure 8 shows the XPS spectra of the Cr 2p core level of glasses (a) T15R and (b) T20R. The measured spectra were corrected by a Shirley background.[21] The binding energies are charge corrected to the C 1s line (285.0 eV). The fits of the spectra show, in addition to the Cr $2p_{3/2}$ line located at 575.7 eV, the presence of another component centered at 578.5 eV. The binding energy values suggest that chromium was present in the two main oxidation states: Cr^{3+} and Cr^{6+}, respectively. The line separation between Cr^{+3} $2p_{1/2}$ and Cr^{+3} $2p_{3/2}$ was 9.7 eV and it was 9.1 eV between Cr^{6+} $2p_{1/2}$ and Cr^{6+} $2p_{3/2}$. The proportion of the Cr^{3+} state in the Cr 2p line was 59% for T15R and 75% for T20R.

These results are in very good agreement with the cromite fraction present in both samples (Fig. 3). That is, when the fraction of Cr crosses the glass dissolution limit, precipitation of cromite takes place, and then a significant fraction of Cr^{6+} is removed from the glassy phase to form cromite crystals; consequently, the content of Cr^{6+} in the T20R sample decreases notably. In this reduction process ($Cr^{6+} \rightarrow Cr^{3+}$), the S present in the starting raw material (Table I) may play an important role.

Based on MAS-NMR and XPS results, Si atoms form chains that are interconnected by trigonal and/or tetragonal borons. In the case of Ca cations, they share oxygen with tetrahedral cations, favoring the interconnection of contiguous chains. In samples with high Ca contents, trigonal and tetrahedral boron are detected, but in samples with increasing amounts of transition metals, the tetrahedral coordination of boron is favored. In general, transition metal atoms form covalent bonds that favor its incorporation into the tetrahedral glass network. This fact can justify the capability of this soda–lime–borosilicate glass to incorporate transition metals into its structure. These metal

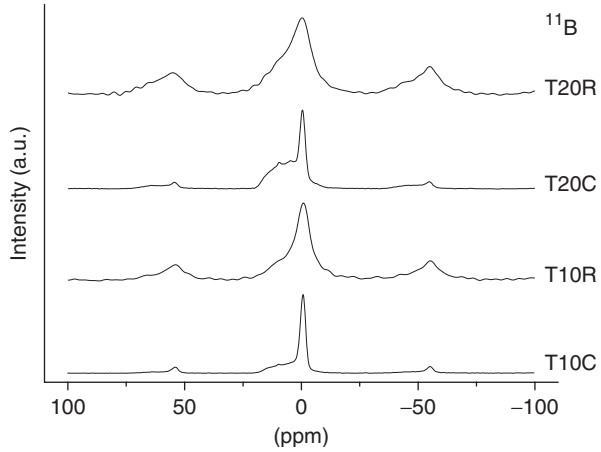

Fig. 7. ^{11}B MAS-NMR spectra for T10C, T10R, T20C, and T20R glasses.

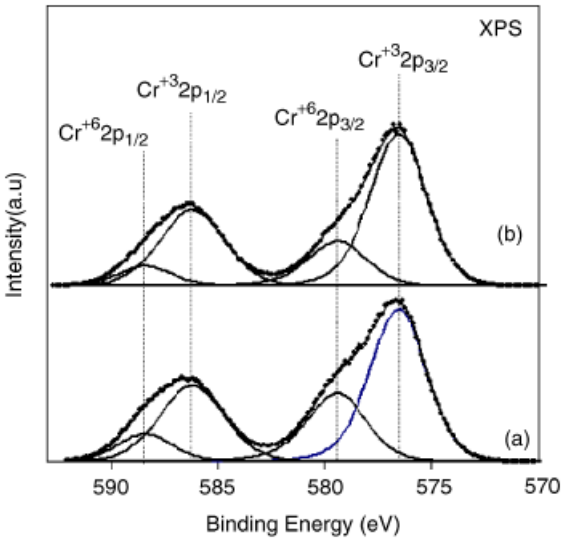

Fig. 8. Cr 2p photoemission spectra of glasses doped with galvanic solid residues: (a) T15R and (b) T20R. The experimental results are represented by dots; the four components of the fit are added as solid curves.

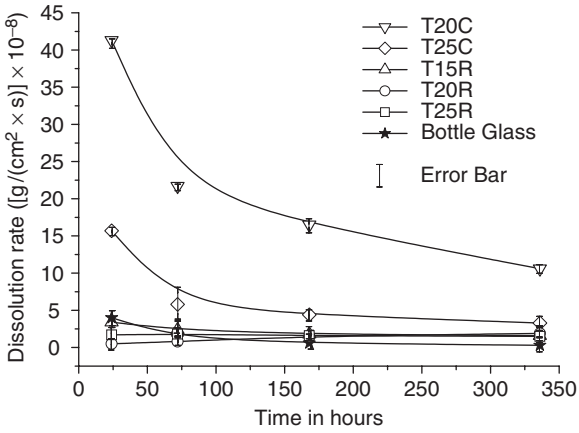

Fig. 9. Resistance to hydrolytic attack versus time for T20C, T25C, T15R, T20R, and T25R glasses and a bottle glass as a reference material.

cations close by bridging the initial open spaces between silica chains, and consequently increase the hydrolytic resistance of the glass. In these glasses, the complete occupation of interstitial sites would impose a limit for the transition metal incorporation, above which phase segregation will be produced.

(2) Chemical Resistance

In Table IV, the ICP analyses of 7 days PCT-B leachate are presented. These results clearly show that the normalized elemental release of T15R, T20R, and T20R glasses is lower than the corresponding PCT specifications for Hanford LAW borosilicate glass for nuclear waste disposal[22] (i.e., 2 g/m^2 for Si and Na and 0.08 g/m^2 for Cr).

In Fig. 9, the mass loss rates produced during the hydrolytic attack of glasses are shown. As a general trend, the hydrolytic resistance increases as the modifier's concentration (CaO or transition metals) increases. The mass loss rate is almost negligible in glasses with a high content of GW, i.e., T15R–T25R.

In agreement with the literature, the chemical stability improves with the modifier content Ca^{2+}.[19] In these glasses, the leaching mechanism[23] is as follows: (i) during the first stages of hydrolytic attack, leaching of alkaline cations (Na, K) from the glass surfaces takes place, and (ii) silica-rich coating layers are subsequently formed that act as a barrier to H_3O^+ diffusion. This fact explains the monotonic decreases of DR curves versus time (Fig. 9). However, silica-rich layers are mechanically unstable and can be removed by spalling. Because of this, the coatings formed cannot be considered to be a permanent protection. Conversely, glasses with a high GW content (T15R, T20R, and T25R) show: (a) a very high hydrolytic resistance ($\leq 2\,[g \cdot (cm^2 \cdot s)^{-1} \times 10^{-8}]$) and (b) a constant DR, similar to the most resistant soda–lime hydrolytic glasses (i.e., bottle glass).

To explain this behavior, we can consider the case of iron-containing glasses. Iron is the most common transition element in silicate glasses and because of this, it has been the subject of numerous studies.[24–28] Holand *et al.*[24] suggested that in the case of SiO_2–Fe_2O_3–NaO glasses studied by XPS, if the concentration of Fe^{3+} is >5 mol%, the Fe^{3+} acts as an intermediate glass former in a manner similar to that of Al^{3+}. This fact is explained considering the corresponding ionic field strengths, z/r (where z is the nominal charge of the ion and r is the ionic radius in nanometer): 56.6 for Al^{3+} and 54.5 for Fe^{3+}. That is, the bonding energy of the O1s core level of atoms bonded to Si and Fe in Si–O–Fe is greater than that in Si–O–Na due to the greater covalence degree of Fe–O bonds. The [FeO_4] polyhedra substitution of [SiO_4] tetrahedral, with Fe^{3+}, must be electrostatically compensated by the Na^+ proximity.

In the case of T15R, T20R, and T25R glasses, the observed chemical stability must be explained considering the higher covalence of the Si–O–(Cr^{3+}, Ni^{2+}, Cu^{2+}) versus Si–O–Na or Si–O–Ca bonding. Then, a closer glass structure is expected in the GW-containing glasses. This fact can explain its observed high hydrolytic resistance behavior. The maximum resistance is attained for T15R; at higher GW contents, cromite is formed. Above this composition, the hydrolytic resistance does not change appreciably (Fig. 9). A similar trend is observed by the PCT-B test (Table IV).

As can be observed in Figs. 3 and 5, crystallization of cromite takes place for T20R. It was also observed by SEM that the hydrolytic attack only occurs in the glassy phase, but not in cromite single-crystal plates (Fig. 10). Then, it is clear that the hydrolytic attack is mainly controlled by the glassy phase resistance. In glasses with a high GW content (T25R), the SO_3 impurity was not totally eliminated during the melting process (Table I and II), probably because of the glass viscosity. In these samples, the SO_3-entrapped gas reacts with NiO and CuO, forming the corresponding insoluble sulfides and creating, by segregation, large spherical shaped inclusions (with a diameter $\geq$1 mm). As described previously, these segregated phases affect the mechanical stability of glasses negatively. Then, considering its chemical and mechanical stability, the optimum glass composition is the one corresponding to T20R. This composition contains $\approx$40 wt% of GW, which was stabilized in the glass matrix.

(3) Viscosity

The viscosity of these glasses (T15R, T20R), corresponding to the shrinkage points (10^{10} dPa · s), softening points ($10^{6.0}$–$10^{7.6}$

Table IV. Normalized Elemental Release (g/m^2) from T15R, T20R, and T25R Glasses after PCT-B Test in Ultra-Pure Water at 90°C for 7 days

Glass	r_{Si}	r_{Ca}	r_{Na}	r_{Cr}	r_{Cu}	r_{Ni}	r_{Zn}
T15R	0.1023	0.0372	0.1550	0.0515	0.0006	0.0022	0.0122
T20R	0.0746	0.0336	0.1396	0.0743	0.0003	0.0016	0.0060
T25R	0.0506	0.0560	0.0922	0.0231	0.0002	0.0005	0.0072

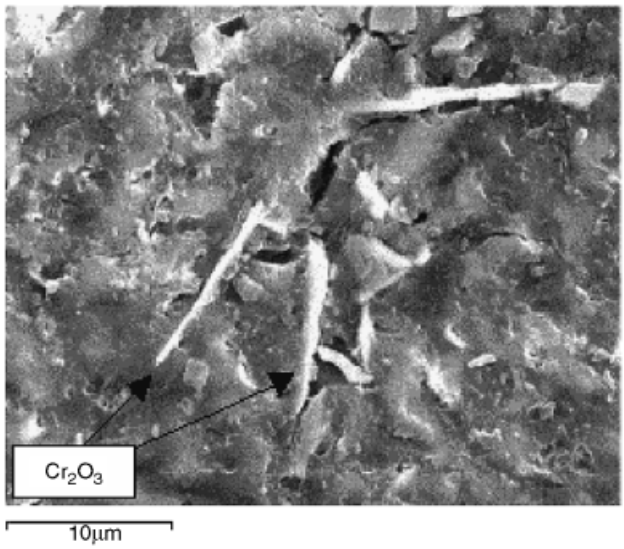

Fig. 10. Scanning electron micrograph corresponding to T20R glass after a 336-h hydrolytic surface attack.

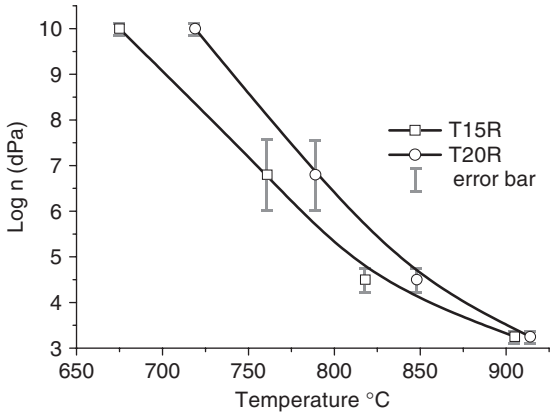

Fig. 11. Viscosity versus temperature curves of T15R and T20R Glasses.

dPa · s), half-ball points ($10^{4.2}$–$10^{4.7}$ dPa · s), and flow points ($10^{3.0}$–$10^{3.5}$ dPa · s)[29,30] was deduced using high-temperature micrographs. This method was used because when crystallization occurs at lower temperatures, the viscosity becomes non-Newtonian and cannot be fit with an Arrhenius equation-based method. In Fig. 11, the temperature dependence of the viscosity is analyzed. As can be observed, these kinds of chemically stable glasses can be cast at a relatively low temperature (<1100°C). This fact is relevant to avoid losses of transition metals (Cr, Ni, Cu, Zn) and consequently the melting/forming further fabrication steps can be considered to be environmental-friendly processes. It is interesting to point out that the viscosity of T20R is higher than that of T15R. This fact can be explained considering the presence of cromite crystallites in the melt (Fig. 5), as can be deduced by Roscoe's equation.[2,31,32]

IV. Conclusions

It has been proved that soda–lime–borosilicate glasses can be used to stabilizes toxic heavy metals (Cr, Ni, Cu, Zn, Pb) of GW up to 40 wt%. The results obtaining clearly indicate that this particular soda–lime–borosilicate glass structure is able to incorporate transition metals, closing by bridging the originally open spaces between silica tetrahedral chains and increasing its hydrolytic resistance to a level similar to bottle glasses.

References

[1]W. E. Lee, A. R. Boccaccini, J. A. Labrincha, C. Leonelli, C. H. III Drummond, and C. R. Cheeseman, "Green Engineering—Ceramic Technology and Sustainable Development," *Am. Ceram. Soc. Bull.*, **86** [2] 18–25 (2007).

[2]D. Huang, C. H. Drummond III, J. Wang, and R. D. Blume, "Incorporation of Chromium(III) and Chromium(VI) Oxides in a Simulated Basaltic, Industrial Waste Glass-Ceramic," *J. Am. Ceram. Soc.*, **87** [11] 2047–52 (2004).

[3]A. Baral, P. Stewart, and R. Engelken, "Chromium-Based Regulations Applicable to Metal Finishing Industries in the United States: A Policy Assessment," *Rev. Pol. Res.*, **23**, 1–21 (2006).

[4]J. M. Magalhaes, J. E. Silva, F. P. Castro, and J. A. Labrincha, "Physical and Chemical Characterisation of Metal Finishing Industrial Wastes," *J. Environ. Manage.*, **75**, 157–66 (2005).

[5]L. Barbieri, A. C. Bonamartini, and I. Lancellotti, "Alkaline and Alkaline–Earth Silicate Glasses and Glasses–Ceramics from Municipal and Industrial Wastes," *J. Eur. Ceram. Soc.*, **20**, 2477–83 (2000).

[6]P. Kavouras, P. Komninou, K. Chrissa, G. Kaimakamis, S. Kokkou, K. Paraskevopoulos, and T. Karakostas, "Microstructural Changes of Processed Vitrified Solid Waste Products," *J. Eur. Ceram. Soc.*, **23**, 1305–11 (2003).

[7]J. Sterpenich and G. Libourel, "Using Stained Glass Windows to Understand the Durability of Toxic Waste Matrices," *Chem. Geol.*, **174**, 181–93 (2001).

[8]G. Roth and S. Weisennburger, "Vitrification of High-Level Level Liquid Waste: Glass Chemistry, Process Chemistry and Process Technology," *Nucl. Eng. Des.*, **202**, 197–207 (2000).

[9]J. Yan and I. Neretnieks, "Is the Glass Phase Rate Always a Limiting Factor in the Leaching Processes of Combustion Residues?," *Sci. Total Environ.*, **172**, 95–118 (1995).

[10]F. M. Eaz-Eldin, "Leaching and Mechanical Properties of Cabal Glasses Developed as Matrices for Immobilization High-Level Wastes," *Nucl. Instrum. Methods Phys. Res.*, **B183**, 285–300 (2001).

[11]A. C. Silva and S. R. H. Mello-Castanho, "Silicate Glasses Obtained from fine Silica Powder Modified with Galvanic Waste Addition," *J. Non-Cryst. Solids*, **348**, 211–7 (2004).

[12]J. Fresner, J. Mair, H. Schnitzer, C. Brunner, G. Gwehenberger, and M. Planasch, "Practical Experiences with the Reduction of the Industrial Use of Water in the Galvanising Industry"; *European Roundtable on Sustainable Consumption and Production*. May 12–14, 2004. Bilbao, Spain.

[13]K. A. Shahid and F. P. Glasser, "Phase Equilibria in the Glass Forming of the System Sodium-Oxide Calcium-Oxide and Silicon-Dioxide," *Phys. Chem. Glasses*, **12** [2] 50–7 (1971).

[14]E. P. Flint and L. S. Wells, "The System Lime-Boric Oxide-Silica," *J. Res. Natl. Bur. Stand.*, **17** [5] 727–52 (1936).

[15]I. M. G. Santos, R. C. M. Moreira, A. G. Souza, R. Lebullenger, A. C. Hernandes, E. R. Leite, C. A. Paskocimas, and E. Longo, "Ceramic Crucibles: A New Alternative for Melting of PbO–BiO1:5–GaO1:5 Glasses," *J. Non-Cryst. Solids*, **319**, 304–10 (2003).

[16]B. C. Sales and L. A. Boatner, "Physical and Chemical Characteristics of Lead-Iron Phosphate Nuclear Waste Glasses," *J. Non-Cryst. Solids*, **79**, 83–116 (1983).

[17]American Society for Testing and Materials (ASTM). *Standard Test Methods for Determining Chemical Durability of Nuclear, Hazardous, and Mixed Waste Glasses: The Product Consistency Test (PCT)*, pp. C1285–97 in ASTM International—Book of Standards, Vol. 12.02 (www.astm.org), 1998.

[18]D. E. Day, Z. Wu, C. S. Ray, and P. Hrma, "Chemically Durable Iron Phosphate Glass Waste Forms," *J. Non-Cryst. Solids*, **241**, 1–12 (1998).

[19]J. M. F. Navarro, *El Vidrio*, 3rd edition, Consejo Superior de Investigaciones Científicas—Fundacion Centro Nacional del Vidrio, Madrid, Spain, 2003 684pp.

[20]K. Friedrich, "Investigation of Layer-Forming Systems," *Met. Erz.*, **11** [5] 160–7 (1914).

[21]M. Aronniemi, J. Sainio, and J. Latineen, "Chemical State Quantification of Iron and Chromium Oxides Using XPS: The Effect of the Background Subtraction Method," *Surf. Sci.*, **578**, 108–23 (2005).

[22]C. W. Kim and D. E. Day, "Immobilization of Hanford LAW in Iron Phosphate Glasses," *J. Non-Cryst. Solids*, **331**, 20–31 (2003).

[23]A. Paul, *Chemistry of Glasses*. Chapman and Hall, Londres, 1982.

[24]D. Holland, A. Mekki, I. A. Gee, C. F. McConville, J. A. Johnson, C. E. Appleyard, and P. M. Thomas, "The Structure of Sodium Iron Silicate Glass—A Multi-Technique Approach," *J. Non-Cryst. Solids*, **253**, 192–202 (1999).

[25]W. E. Jackson, F. Farges, M. Yeager, P. A. Mabrouk, S. Rossano, G. A. Waychunas, E. I. Solomon, and G. E. Jr. Brown, "Multi-Spectroscopic Study of Fe(II) in Silicate Glasses: Implications for the Coordination Environment of Fe(II) in Silicate Melts," *Geochim. Cosmochim. Acta*, **69** [17] 4315–32 (2005).

[26]F. Farges, Y. Lefrere, S. Rossano, A. Berthereau, G. Calas, and G. E. Jr. Brown, "The Effect of Redox State on the Local Structural Environment of Iron in Silicate Glasses: A Combined XAFS Spectroscopy, Molecular Dynamics, and Bond Valence Study," *J. Non-Cryst. Solids*, **344**, 176–88 (2004).

[27]S. Rossano, F. Farges, A. Ramos, J. M. Delaye, and G. E. Jr. Brown, "Bond Valence in Silicate Glasses," *J. Non-Cryst. Solids*, **304**, 167–73 (2002).

[28]S. Rossano, A. Y. Ramos, and J. M. Delaye, "Environment of Ferrous Iron in $CaFeSi_2O_6$ Glass; Contributions of EXAFS and Molecular Dynamics," *J. Non-Cryst. Solids*, **273**, 48–52 (2000).

[29]H. Scholze, "Influence of Viscosity and Surface Tension on Hot-Stage Microscopy Measurements on Glasses," *Ver. Dtsch Keram. Ges.*, **391**, 63–8 (1962).

[30]A. De Pablos, A. Duran, and M. I. Nieto, "Adjusting of Laboratory Filature Furnace for Obtaining Fiberglass," *Bol. Soc. Esp. Ceram. Vidr.*, **36**, 517–23 (1997).

[31]Y. Bottinga and D. F. Weill, "The Viscosity of Magmatic Silicate Liquids: A Model for Calculation," *Am. J. Sci.*, **272**, 438–75 (1972).

[32]R. Roscoe, "The Viscosity of Suspensions of Rigid Sphere," *Br. J. Appl. Phys.*, **3**, 267–9 (1952). □